minerals

MDPI

Article

Stability Analysis of Cemented Tailings Backfill in Stope Considering Layered Structural Characteristics

Jie Wang [1,*], Qingjun Yu [2], Guannan Wang [2] and Dazhi Tong [2]

[1] School of Civil and Resource Engineering, University of Science and Technology Beijing, Beijing 100083, China
[2] Chifeng Shanjin Hongling Nonferrous Mining Co., Ltd., Chifeng 025454, China; yuqj@sd-gold.com (Q.Y.); wangguannan@sd-gold.com (G.W.); tongdazhi@sd-gold.com (D.T.)
* Correspondence: wangjie123@ustb.edu.cn

Abstract: In this study, the stage subsequent to filling mining is selected as the background, and the cemented tailings backfill serves as the research object. Given the effects of the layer effect, top load, lateral pressure coefficient, and so forth, a safety factor calculation model of cemented tailings backfill in large depth–width ratio stopes is developed in accordance with the Mohr–Coulomb failure criterion, which is compared with the models proposed by other scholars. Lastly, the characteristics of the effect exerted by a wide variety of factors are discussed. As indicated by the results, (1) there are three scenarios in the position of the sliding surface, located in the first layer, passing through two layers and passing through three layers, and mainly the first two. Compared with other models, the rationality and reliability of the model in this study are verified. Different models have different research backgrounds and different focuses, and certain differences exist in results. (2) The safety factor of cemented tailings backfills is reduced with the increase of the top load, the lateral pressure coefficient, and the bulk density, while it is increased with the increase of cohesion, internal friction angle, and bonding force ratio. Furthermore, a linear functional relationship exists between them. The safety factor has the maximum sensitivity to cohesion and the minimum sensitivity to top load. (3) Using Statistical Package for the Social Sciences (SPSS) software for regression analysis, a simplified multiple linear regression equation between the safety factor and the respective factor is built. The regression results achieve an error of 10%. As revealed by the result of this study, the simplified regression equation can be applied to the stability evaluation of the on-site cemented tailings backfill.

Keywords: subsequent filling; cemented tailings backfill; layer effect; safety factor; stability analysis

Citation: Wang, J.; Yu, Q.; Wang, G.; Tong, D. Stability Analysis of Cemented Tailings Backfill in Stope Considering Layered Structural Characteristics. *Minerals* **2023**, *13*, 1111. https://doi.org/10.3390/min13091111

Academic Editor: Ferdi Cihangir

Received: 5 July 2023
Revised: 14 August 2023
Accepted: 15 August 2023
Published: 22 August 2023

1. Introduction

The filling method refers to a mining method that mixes solid waste (e.g., waste rock and tailings) that is generated from ore mining with cement and water in a certain proportion before backfilling to the goaf [1–3]. This method shows several significant advantages (e.g., high safety and green environmental protection), and it has been increasingly applied on a year-to-year basis. The method of sublevel open stoping with subsequent filling refers to an organic integration of the open-stoping method and the filling method. It combines the high efficiency and low cost of the open-stoping method, as well as the safety and environmental protection of the filling method, representing the development direction of future large-scale green mining [4–6].

In general, the sublevel open stoping with subsequent filling method divides the stope into rooms and pillars. The first step is to mine the room and then use tailings cementation to fill the goaf in rooms. The filling process comprises three steps as follows [7–9]. First, a high cement–sand ratio slurry is employed to fill the bottom of the goaf in the room to form higher bottom strength [10–12]. Subsequently, a slurry with a relatively low cement–sand ratio is adopted to fill the middle of the goaf in the rooms, with the aim of lowering filling

costs. Lastly, the top of the goaf in the rooms is filled with a high cement–sand ratio slurry again, thus reducing the settlement of the backfill to facilitate roof connection while serving as a top pillar mining platform. The second step refers to mining adjacent pillars and then filling the goaf in the pillars with non-cemented waste rock or tailings. When only one side of the goaf adjacent to the cemented backfill is filled, one side of the cemented backfill turns out to be empty, while the other side is subjected to lateral pressure from the adjacent non-cemented backfill. On that basis, the stress state and stability of the cemented backfill are the worst, and the risk of sliding instability and failure is the highest. Accordingly, the research on the stress characteristics and stability status of the cemented backfill takes on great practical significance.

The theoretical research on the stability of cemented fill materials in mining areas worldwide was initiated in the 1980s. L. Li and M Aubertin et al. [13–15] built a small aspect ratio stability evaluation model for cemented backfill based on the Mohr–Coulomb failure criterion but did not consider the layering effect of cemented backfill. Mitchell et al. [16,17] proposed a safety factor analytical calculation model based on the limit equilibrium method for the scenario where one side of the cemented backfill is empty. This model considers the contact bonding effect between the cemented backfill and the surrounding rock, whereas the back wall is the surrounding rock, and the cemented backfill is not subjected to lateral pressure. Liu et al. [18,19] proposed four 3D analytical models and methods in terms of the safety coefficient and strength requirements of cemented backfill without considering the layering effect of cemented backfill. Zhang et al. [20] considered the effect of filling sequence and top overload and built a unified solution model for sliding instability of cemented backfill. However, Zhang et al. believed that cemented backfill is subject to the upward bonding force of the non-cemented backfill on the back wall. Smith et al. [21] considered the effect of the dip angle of the ore body and proposed a strength demand model for unilateral exposure of inclined cemented backfill, and derived an equation for calculating the safety factor of unilateral exposure of inclined cemented backfill. Liu et al. [22] studied the effect of lateral pressure on the stability of cemented fill materials based on the mining and filling time sequence of sublevel open stoping with subsequent filling methods and revised the analytical model and method for the strength requirement of cemented fill materials.

As revealed by the above-mentioned research, the strength models of cementitious backfill constructed by different scholars have different research backgrounds and consider certain differences in factors. Moreover, the layering effect of cemented backfill is usually not considered, and the presence of layering can change the internal stress distribution state of the backfill, degrade the overall strength of the backfill, and thus affect the determination of sliding instability. However, layering filling can greatly reduce the filling cost.

After the filling process is precisely controlled, the layered filling is gradually facilitated and applied at subsequent stages. The strength model for the complete filling body is no longer suitable for mining needs, so it is necessary to construct a stability judgment model suitable for layered cemented backfill. Thus, in accordance with the Mohr–Coulomb failure criterion, this study focuses on the layered cemented backfill as the research object. By taking into account the effects of stratification, top load, lateral pressure coefficient, and other factors, a safety factor solution model for layered cementitious filling with front wall exposure and rear wall compression is built, and the reasonable reliability of the model was verified, the impact of a wide variety of factors on the safety factor was explored, and simplified regression processing of complex models using SPSS software [23,24] was used to provide certain theoretical guidance for on-site applications.

2. Construction of a 3D Strength Model for Layered Backfill

The rooms and pillars in the mining area are extracted in steps, with one step mining the rooms and then using tailings cemented backfill to fill the goaf in the room. In general, to save filling costs, the layered filling is employed; the cemented filling of the room displays a three-layer structure, exhibiting a higher proportion of bottom and top layers and a lower proportion of middle layers. The two-step mining of adjacent pillars is basically completed

with non-cemented filling. When one side of the pillar goaf is filled, whereas the other side of the pillar goaf is not yet filled (Figure 1), the layered cemented backfill is affected by both the self-weight stress and the lateral pressure of adjacent non-cemented backfill. As a result, the layered cemented backfill exhibits the worst stability. Studying the stress characteristics of the layered cemented backfill at this time takes on critical significance in regulating the structure of the layered backfill and increasing the filling ratio.

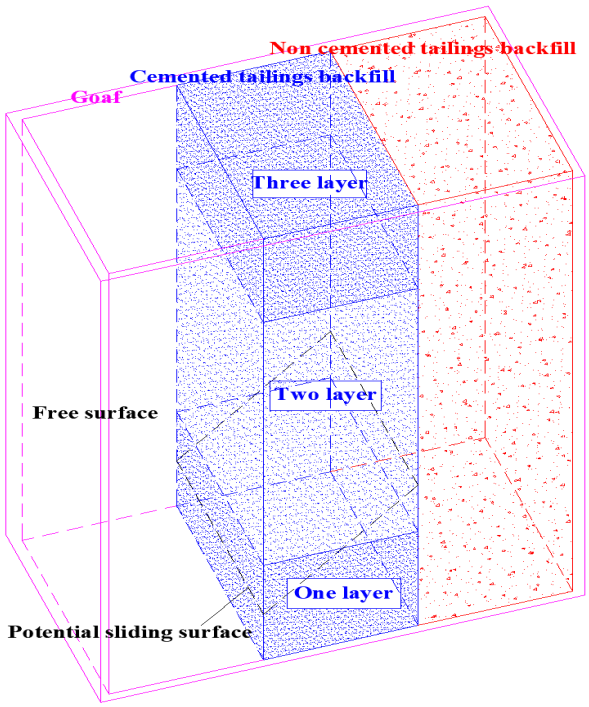

Figure 1. Occurrence state of layered cemented tailings backfill.

2.1. Basic Assumptions

During the force analysis, reasonable assumptions should be made regarding the model, which simplifies the calculation while showing greater consistency with the practical scenario on site. In accordance with the research of L. Li and Zhang et al. [13,20], this study makes the following basic assumptions:

(1) In general, the cementitious filling bodies display a three-layer structure, which falls into one, two, and three layers from top to bottom, with equal heights at the top and bottom;
(2) The first and third layers comprise a false top and false bottom structure with identical proportions and mechanical parameters;
(3) The internal friction angles of the three layers are identical;
(4) Without considering the sliding friction effect between layered cemented backfill and rocks on both sides, it is assumed that the bond–slip effect only exists between them [14,25,26];
(5) The layered cemented backfill undergoes failure along an inclined sliding surface, and the inclination angle of the sliding surface is determined based on the Rankine active earth pressure failure surface;
(6) The lateral pressure of the non-cemented backfill on the rear wall is the self-weight stress multiplied by the lateral pressure coefficient: $v\gamma_u h$;
(7) Shear strength of backfill τ.

Conforming to the Mohr–Coulomb criterion, it is expressed as

$$\tau = c + \sigma \tan \varphi \quad (1)$$

where σ denotes the normal force acting on the sliding surface; c is the cohesion of backfill; φ is the friction angle of backfill; v is the lateral pressure coefficient of non-cemented backfill, $v = \tan^2(45 - \frac{\varphi}{2})$ [27]; and γ_u expresses the unit weight of non-cemented backfill.

The mechanical parameters of the respective part are set, as shown in Figure 1. To be specific, H, B, and L represent the height, width, and length of the layered cemented backfill; P_0 denotes the uniformly distributed load on the top of the layered cemented backfill; h_1 represents the thickness of the first and third layers; h_2 represents the thickness of the second layer; and h_c expresses the distance between the slope bottom (the height between the sliding surface slope bottom and the bottom of stope). γ_1 and c_1 represent the bulk density and cohesion of the first and third layers of the cemented filling body. γ_2 and c_2 represent the bulk density and cohesion of the second layer of the cemented filling body. $c_{1'}$ is the bonding force between the first and third layered cemented backfill and the surrounding rock of the sidewall. $c_{2'}$ expresses the bonding force of the second layer cemented backfill and the surrounding rock of the sidewall, And the bonding force is usually proportional to the cohesion within the cemented backfill, which is affected by the roughness of the contact surface, $c_{1'} = r_1 c_1$, $c_{2'} = r_2 c_2$, $r_1 \in [0, 1]$, $r_2 \in [0, 1]$, $r_1 = r_2$. α denotes the angle between the sliding surface and the horizontal plane, $\alpha = 45° + \varphi/2$, because it is assumed that the internal friction angle of the respective part of the cemented backfill is the same, and the sliding surface is located in the same plane.

h_c, B and α are the three variables that determine the positional relationship of the sliding surface, which can be divided into three scenarios based on the intersection relationship between the sliding surface and each sublayer. First, the sliding surface is located in a layered layer, $D = h_c + B\tan\alpha \leq h_1$, and D denotes the distance between the top of the slope (the height of the sliding surface from the top of the slope to the bottom of the stope). Second, the sliding surface passes through the first and second layers, $h_1 \leq h_c + B\tan\alpha \leq h_1 + h_2$. Third, the sliding surface passes through three layers, $h_1 + h_2 \leq h_c + B\tan\alpha \leq H$. The specific discussions on these three scenarios are presented as follows.

2.2. The Sliding Surface Is Located in the First Layer

When the sliding surface is completely located in a layer, the structural characteristics of stope are shown in Figure 2, $h_c + B\tan\alpha \leq h_1$.

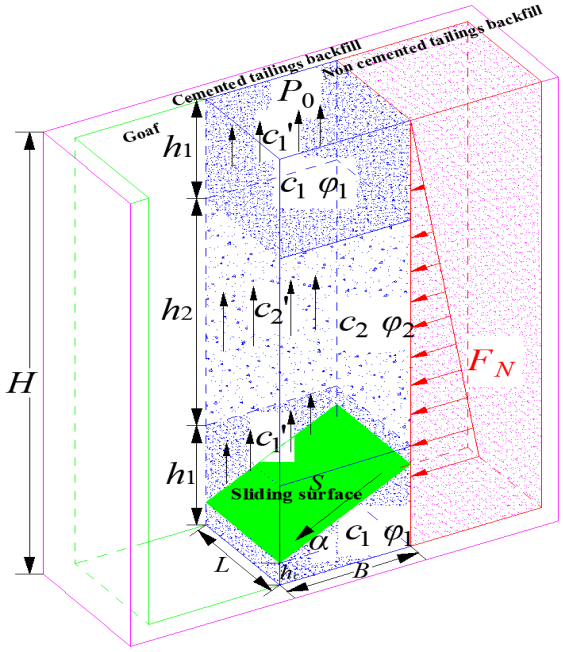

Figure 2. The sliding surface is located in the first layer of cemented tailings backfill.

It is assumed that the roughness of rock on both sides is consistent and consistent with the bonding effect of the cemented backfill:

$$\begin{cases} f_1 = c_1' B(2h_1 - h_c - B\tan\alpha) \\ f_2 = 2c_2' BH_2 \\ f_3 = 2c_1' BH_1 \end{cases} \quad (2)$$

The total friction force is

$$f = 2c_1' Bh_1 + 2c_2' Bh_2 + c_1' B(2h_1 - h_c - B\tan\alpha) \quad (3)$$

The lateral pressure acting on the back wall of the non-cemented backfill is assumed as F_N, which is expressed as

$$F_N = \int_0^{H'} v\gamma_u hLdh = \frac{1}{2} v\gamma_u L(H - h_c - B\tan\alpha)^2 \quad (4)$$

T denotes the sum of the self-gravity of a wedge-shaped sliding body and the uniform force acting on its top, which is expressed as

$$T = p_0 BL + \gamma_1 LBh_1 + \gamma_2 LBh_2 + \frac{1}{2}\gamma_1 LB(2h_1 - h_c - B\tan\alpha) \quad (5)$$

In accordance with the principle of force balance, the combined forces M and N of the vertical sliding surface and the downward sliding surface of the wedge-shaped sliding body are expressed as follows:

$$\begin{cases} M = (T - f)\cos\alpha - F_N \sin\alpha \\ N = (T - f)\sin\alpha + F_N \cos\alpha \end{cases} \quad (6)$$

Following the Mohr–Coulomb criterion, the anti-slip force K of a wedge-shaped sliding body is denoted as

$$K = (c_1 + \frac{M\cos\alpha}{BL}\tan\varphi)BL/cos\alpha \quad (7)$$

The safety factor F of the cemented backfill represents the ratio of anti-sliding force K to sliding force N, which is written as

$$F = \frac{K}{N} = \frac{(c_1 + \frac{M\cos\alpha}{BL}\tan\varphi)BL/cos\alpha}{N} \quad (8)$$

2.3. Sliding Surface Passing through Two Layers

The structural characteristics of the mining area are presented in Figure 3 when the sliding surface passes through the first and second layers. At this time, $h_1 < h_c + B\tan\alpha \leq h_1 + h_2$.

The frictional forces of the surrounding rock on both sides of the wedge-shaped sliding body are written as

$$\begin{cases} f_1 = \frac{c_1'(h_1 - h_c)^2}{\tan\alpha} \\ f_2 = \frac{2c_2'(h_1 - h_c)h_2}{\tan\alpha} + c_2'(h_1 + 2h_2 - h_c - B\tan\alpha)(B - \frac{h_1 - h_c}{\tan\alpha}) \\ f_3 = 2c_1' BH_1 \end{cases} \quad (9)$$

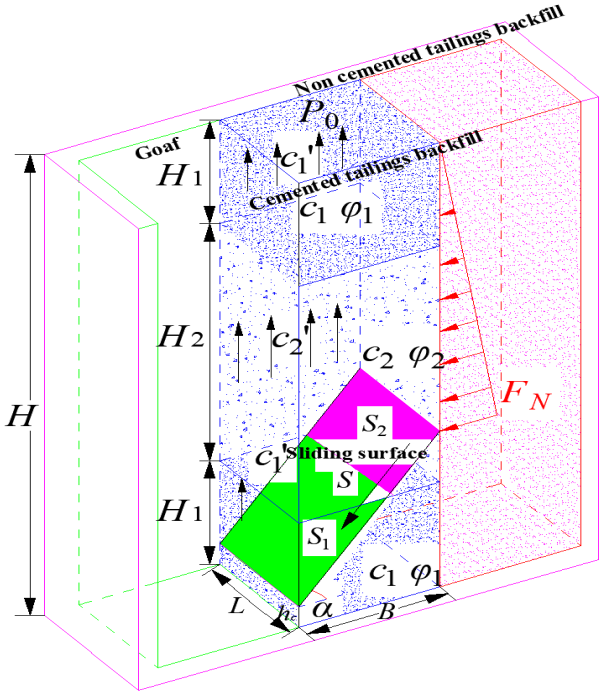

Figure 3. The sliding surface passes through the first and second layers of cemented tailings backfill.

The total friction force is expressed as

$$f = 2c_1'Bh_1 + \frac{2c_2'(h_1 - h_c)h_2}{\tan\alpha} + c_2'(h_1 + 2h_2 - h_c - B\tan\alpha)(B - \frac{h_1 - h_c}{\tan\alpha}) + \frac{c_1'(h_1 - h_c)^2}{\tan\alpha} \quad (10)$$

The lateral pressure acting on the cemented backfill by the non-cemented backfill on the back wall is

$$F_N = \int_0^{H'} v\gamma_u hLdh = \frac{1}{2}v\gamma_u L(H - h_c - B\tan\alpha)^2 \quad (11)$$

The sum of the self-gravity and the top uniformly distributed load of the wedge-shaped sliding body is defined as

$$T = P_0BL + \gamma_1 BLh_1 + \frac{\gamma_1 L(h_1 - h_c)^2}{2\tan\alpha} + \frac{\gamma_2 L(h_1 - h_c)h_2}{\tan\alpha} + \frac{\gamma_2 L}{2}(h_1 + 2h_2 - h_c - B\tan\alpha)(B - \frac{h_1 - h_c}{\tan\alpha}) \quad (12)$$

In accordance with the principle of force balance, the wedge-shaped sliding body is subjected to the combined force of the vertical sliding surface and the downward sliding surface as follows:

$$\begin{cases} M = (T - f)\cos\alpha - F_N\sin\alpha \\ N = (T - f)\sin\alpha + F_N\cos\alpha \end{cases} \quad (13)$$

The anti-slip force of the wedge-shaped sliding body is written as

$$K = (\frac{M}{S}\tan\varphi + c_1)S_1 + (\frac{M}{S}\tan\varphi + c_2)S_2 \quad (14)$$

To be specific,

$$\begin{cases} S = \frac{BL}{\cos\alpha} \\ S_1 = \frac{L(h_1 - h_c)}{\sin\alpha} \\ S_2 = (\frac{B}{\cos\alpha} - \frac{h_1 - h_c}{\sin\alpha})L \end{cases} \quad (15)$$

Likewise, the safety coefficient of the cemented backfill can be obtained as follows:

$$F = \frac{K}{N} = \frac{(\frac{M}{S}\tan\varphi + c_1)S_1 + (\frac{M}{S}\tan\varphi + c_2)S_2}{N} \tag{16}$$

2.4. Sliding Surface Passing through Three Layers

The structural characteristics exhibited by the stope are illustrated in Figure 4 when the sliding surface passes through three layers. To be specific, there are $h_1 + h_2 < h_c + B\tan\alpha \leq H$.

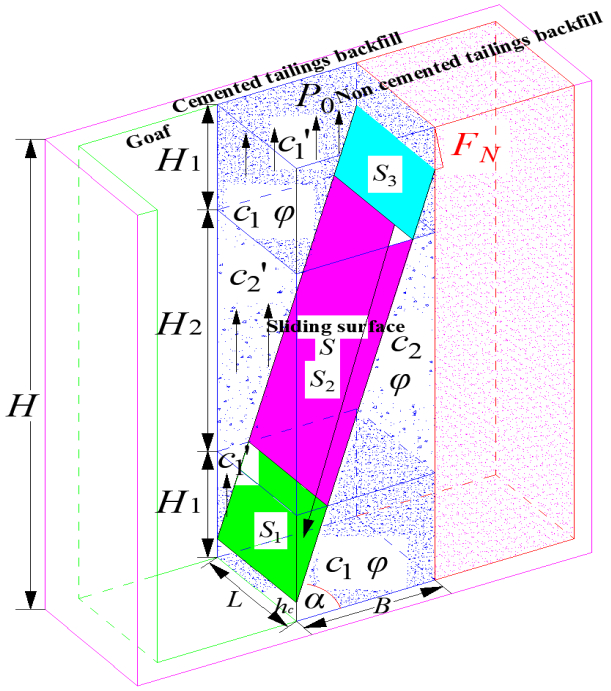

Figure 4. The sliding surface passes through three layers of cemented tailings backfill.

The frictional forces of the surrounding rocks on both sides of the wedge-shaped sliding body are expressed as

$$\begin{cases} f_1 = \frac{c_1'(h_1 - h_c)^2}{\tan\alpha} \\ f_2 = c_2' h_2 \frac{H - 2h_c}{\tan\alpha} \\ f_3 = (2Bh_1 - \frac{(B\tan\alpha + h_c - h_1 - h_2)^2}{\tan\alpha})c_1' \end{cases} \tag{17}$$

The total friction force is written as

$$f = \frac{c_1'(h_1 - h_c)^2}{\tan\alpha} + c_2' h_2 \frac{H - 2h_c}{\tan\alpha} + (2Bh_1 - \frac{(B\tan\alpha + h_c - h_1 - h_2)^2}{\tan\alpha})c_1' \tag{18}$$

The lateral pressure acting on the cemented backfill by the non-cemented backfill on the back wall is

$$F_N = \int_0^{H'} v\gamma_u h L dh = \frac{1}{2} v\gamma_u L(H - h_c - B\tan\alpha)^2 \tag{19}$$

The self-gravity and uniformly distributed force load on the top of the wedge-shaped sliding body are expressed as

$$T = P_0 BL + \frac{\gamma_1 L(h_1 - h_c)^2}{2\tan\alpha} + \frac{\gamma_2 L h_2 (H - 2h_c)}{2\tan\alpha} + \gamma_1 L[Bh_1 - \frac{(B\tan\alpha + h_c - h_1 - h_2)^2}{2\tan\alpha}] \tag{20}$$

The combined force of the vertical sliding surface and the downward sliding surface of the wedge-shaped sliding body is

$$\begin{cases} M = (T - f)\cos\alpha - F_N \sin\alpha \\ N = (T - f)\sin\alpha + F_N \cos\alpha \end{cases} \tag{21}$$

The anti-slip force of a wedge-shaped sliding body is

$$K = (\frac{M}{S}\tan\varphi_1 + c_1)S_1 + (\frac{M}{S}\tan\varphi_2 + c_2)S_2 + (\frac{M}{S}\tan\varphi_1 + c_1)S_3 \tag{22}$$

To be specific,

$$\begin{cases} S = \frac{BL}{\cos\alpha} \\ S_1 = \frac{L(h_1 - h_c)}{\sin\alpha} \\ S_2 = \frac{Lh_2}{\sin\alpha} \\ S_3 = \frac{LB}{\cos\alpha} - \frac{L(h_1 + h_2 - h_c)}{\sin\alpha} \end{cases} \tag{23}$$

The safety factor of the cemented backfill is defined as

$$F = \frac{K}{N} = \frac{(\frac{M}{S}\tan\varphi_1 + c_1)S_1 + (\frac{M}{S}\tan\varphi_2 + c_2)S_2 + (\frac{M}{S}\tan\varphi_1 + c_1)S_3}{N} \tag{24}$$

2.5. Model Validation

The strength models of filling materials built by different scholars have a wide variety of research backgrounds, such that the focus and considerations turn out to be different as well. The safety factor of the model in this study is compared with the results of other scholars. The parameters are taken based on Table 1, and the results are illustrated in Figure 5.

Table 1. Value of each factor.

Factor	Top Load P0/(KN)	Lateral Pressure Coefficient v	Bottom Cohesion c_1/(MPa)	Central Cohesion c_2/(MPa)	Bottom Bulk Density γ_1/(KN·m^{-3})	Central Bulk Density γ_2/(KN·m^{-3})	Bond Force Ratio $r_1 = r_2$	Internal Friction Angle φ/(°)
Top load P0/(KN)	VAR	0.2	0.36	0.3	22	20	0.6	30
lateral pressure coefficient v	50	VAR	0.36	0.3	22	20	0.6	30
Bottom cohesion c_1/(MPa)	50	0.2	VAR	0.3	22	20	0.6	30
Central cohesion c_2/(MPa)	50	0.2	0.36	VAR	22	20	0.6	30
Bottom bulk density γ_1/(KN·m^{-3})	50	0.2	0.36	0.3	VAR	20	0.6	30
Central bulk density γ_2/(KN·m^{-3})	50	0.2	0.36	0.3	22	VAR	0.6	30
Bond force ratio $r_1 = r_2$	50	0.2	0.36	0.3	22	20	VAR	30
internal friction angle φ/(°)	50	0.2	0.36	0.3	22	20	0.6	VAR

Note: VAR represents a variable. VAR$_{P0}$ = 0, 50, 100, 150, 200, 250 KN; VAR$_v$ = 0.16, 0.18, 0.20, 0.22, 0.24, 0.26; VARc_1 = 0.33, 0.34, 0.35, 0.36, 0.37, 0.38 MPa; VARc_2 = 0.28, 0.29, 0.30, 0.31, 0.32, 0.33 MPa; VARγ_1 = 20, 21, 22, 23, 24, 25 KN/m^3; VARγ_2 = 16, 17, 18, 19, 20, 21 KN/m^3; VAR$r_2 = r_2$ = 0.45, 0.50, 0.55, 0.60, 0.65, 0.70; VARφ = 28°, 29°, 30°, 31°, 32°, 33°.

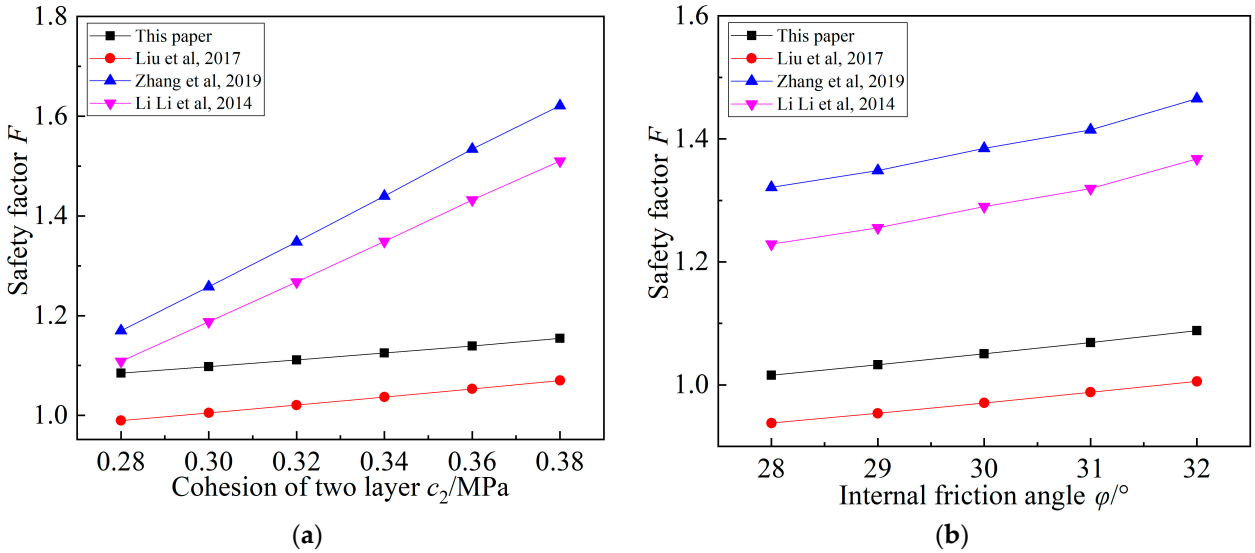

Figure 5. Comparison of safety factors of different models [15,19,20]. (**a**) Safety factor and cohesion; (**b**) Safety and internal friction angle.

As depicted in Figure 5, the safety coefficients of all models are elevated with the increase of the central cohesion and the internal friction angle. With the rise of cohesion, the bonding strength between the fine particles of the cemented backfill is increased. Moreover, the tensile and shear resistance of particles, the overall resistance to failure, and the safety factor are all increased. With the increase of the internal friction angle, the friction coefficient between particles shows an equivalent increase, and the particle shear resistance, the overall failure resistance, and the safety factor are generally increased.

To be specific, the model proposed by Zhang et al. [20] has the highest safety factor, as it takes into account the upward friction force of the non-cemented backfill on the back wall against the cemented backfill. The combined force of the wedge sliding body increases upwards, and the downward sliding trend weakens, resulting in a corresponding increase in safety factor; However, Li et al. [13] ignored the lateral pressure of the non-cemented backfill on the rear wall, which is equivalent to reducing the downward force of the wedge-shaped sliding body and increasing the safety factor. The model proposed by Liu et al. [19] suggests that the foot of the sliding surface slope is located at the bottom of the stope, which increases the downward force of the wedge-shaped sliding body, resulting in a lower safety factor compared with this study.

3. Analysis of Sliding Instability of Layered Cemented Backfill

3.1. Determination of Sliding Surface Position

The previous analysis suggests that the position of the sliding surface is determined by the width B of the room, the distance between the slope bottom h_c, as well as the inclination angle of the sliding surface α. To be specific, α is also correlated with the friction angle within the cemented backfill, such that it can be determined in accordance with B, h_c, and φ. The three determine the position of the sliding surface, whereas the values of other parameters are still consistent with those listed in Table 1 below, as presented in Figure 6.

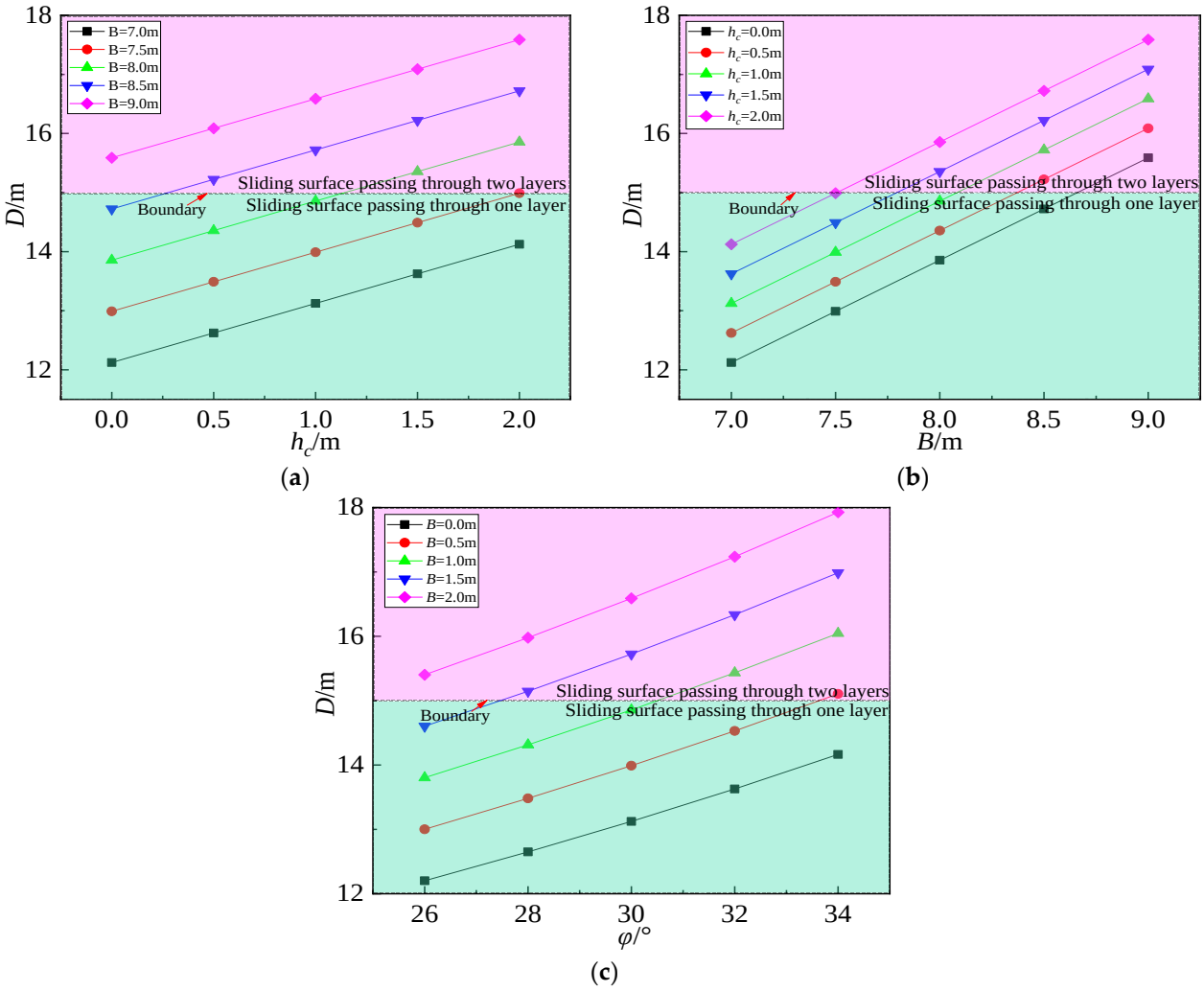

Figure 6. The relationship between the position of the sliding surface and h_c, B, and φ. (**a**) D and h_c; (**b**) D and B; (**c**) D and φ.

Figure 6 illustrates the correlation curve between the position of the sliding surface and the three factors. As depicted in Figure 6a, the distance h_d from the top of the slope will be increased with the rise of the distance h_c from the bottom of the sliding surface slope. When the width of the room is small and the distance between the slope and the bottom varies between 0–2 m, the sliding surface is always within a layer. When the width of the mining room increases to 8 m and the slope bottom distance is small, the sliding surface is located in the first layer. When the slope bottom distance is large, the sliding surface will pass through the first layer to reach the second layer. When the width of the mining room is increased to over 9 m, the position of the sliding surface is no longer affected by the slope bottom distance and always runs through the first and second layers. As depicted in Figure 6b, the top distance of the sliding surface is increased with the increase of the room width. And regardless of how the bottom distance caries, the curve passes through the boundary of the first and second layers. In other words, the sliding surface will pass through the two layers when the room width is increased to a certain extent. As revealed by the above conclusion, the effect of the room width on the position of the sliding surface exceeds the bottom distance of the slope. Figure 6c present the correlation between the position of the sliding surface and the friction angle within the cemented backfill. As depicted in the figures, the friction angle within the cemented backfill also notably affects the position of the sliding surface. The distance between the top of the sliding surface slope will be increased with the rise of the internal friction angle. Under the small width

B of the room and the small distance h_c between the slope bottom, regardless of how the internal friction angle is increased, the sliding surface is constantly located in one layer. Nevertheless, under the large distance h_c between room B and the slope bottom, the sliding surface tends to move up till passing through the two layers.

The above analysis suggests that the position of the sliding surface will vary between the first and second layers, and it cannot pass through all three layers simultaneously. If the sliding surface should pass through three layers simultaneously, the distance hd from the top of the slope must exceed the sum of the heights of the two layers at the bottom. In general, the internal friction angle of backfill φ is nearly 30°, and there will be no significant increase. Nevertheless, the sliding surface slope bottom is generally located at the bottom, suggesting that the slope bottom distance h_c is usually 0. Thus, the width B of the room should be sufficiently large. On that basis, the cemented backfill does not conform to the large aspect ratio mechanical model, and its failure mode is no longer shear failure along the sliding surface. The above mechanical model is no longer applicable.

Figure 7 shows the correlation between slope toe distance and safety factor. As depicted in the figure, slopes toe distance affects safety factors to a certain extent. When the slope toe distance is small (at which point the sliding surface is located in a layer), the safety factor increases with the increase of slope toe distance; when the distance between the foot of the slope increases to a certain value (the sliding surface passes through two layers), the safety factor no longer continues to increase. And the minimum safety factor occurs when the slope toe distance is 0; that is, when the sliding surface intersects with the bottom of the stope, the sliding body is the most unstable.

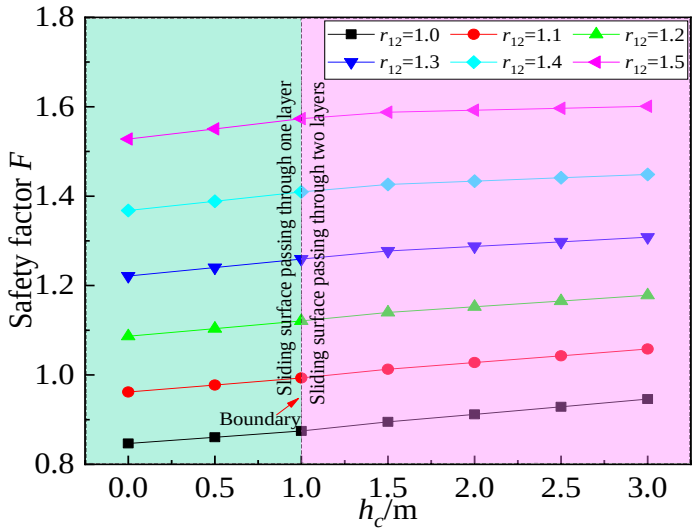

Figure 7. Relationship between toe distance and safety factor.

3.2. Safety Factor Analysis

As indicated by the previous analysis, when the foot distance of the wedge-shaped sliding body is 0, the sliding trend of the sliding body turns out to be more significant, and the sliding body exhibits minimum stability. Accordingly, studying the stability of the sliding body at this time takes on critical significance. The control variates are used to analyze the effect of a variable on the safety factor of the sliding body, keeping other variables unchanged and changing only a single variable. Table 1 lists the values of the respective factor, and Figures 8–11 illustrate the analysis results.

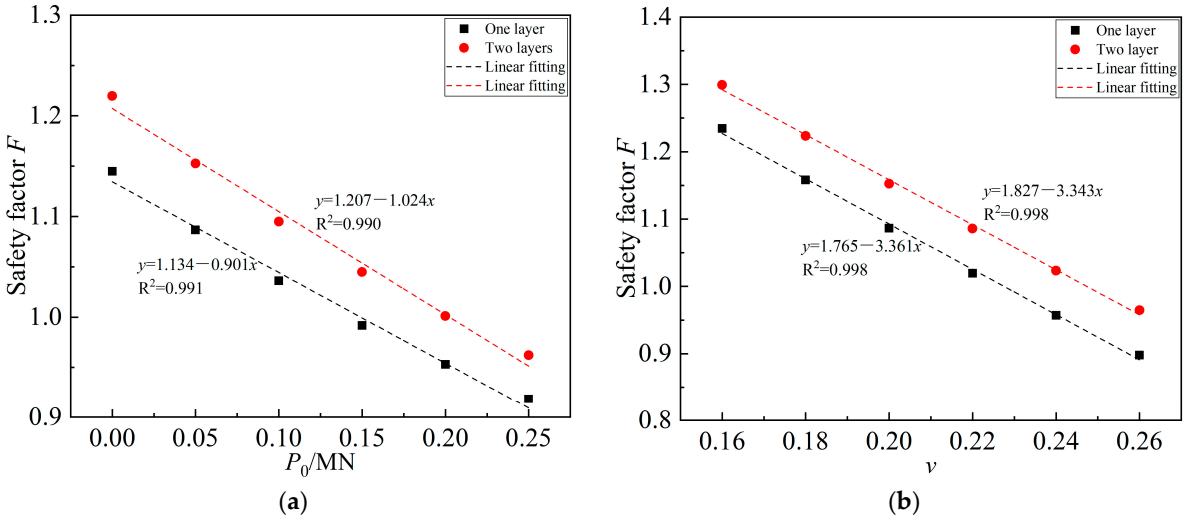

Figure 8. Relationship between safety factor and top load and lateral pressure coefficient. (**a**) Safety and top load; (**b**) Safety and lateral pressure coefficient.

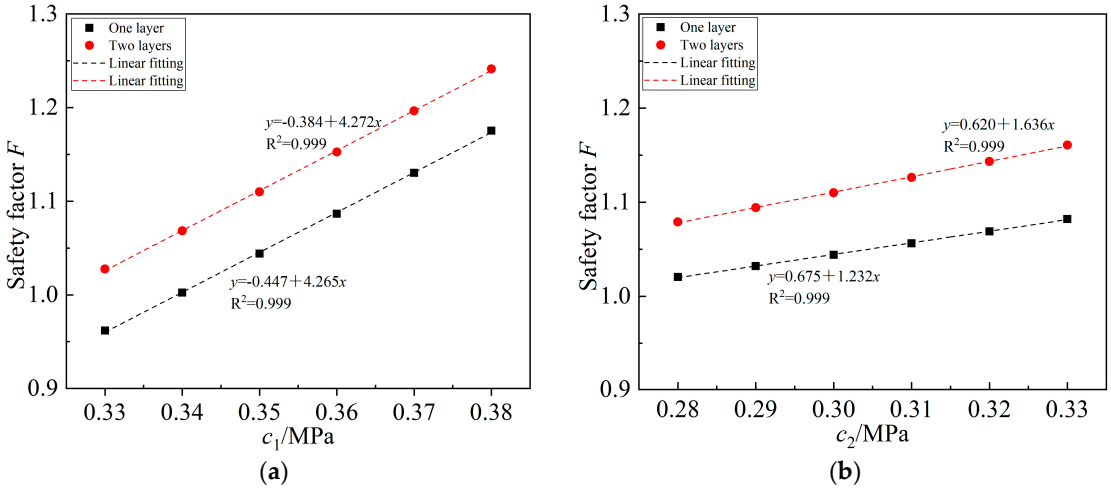

Figure 9. Relationship between safety factor and cohesion. (**a**) Safety and bottom cohesion; (**b**) Safety and central cohesion.

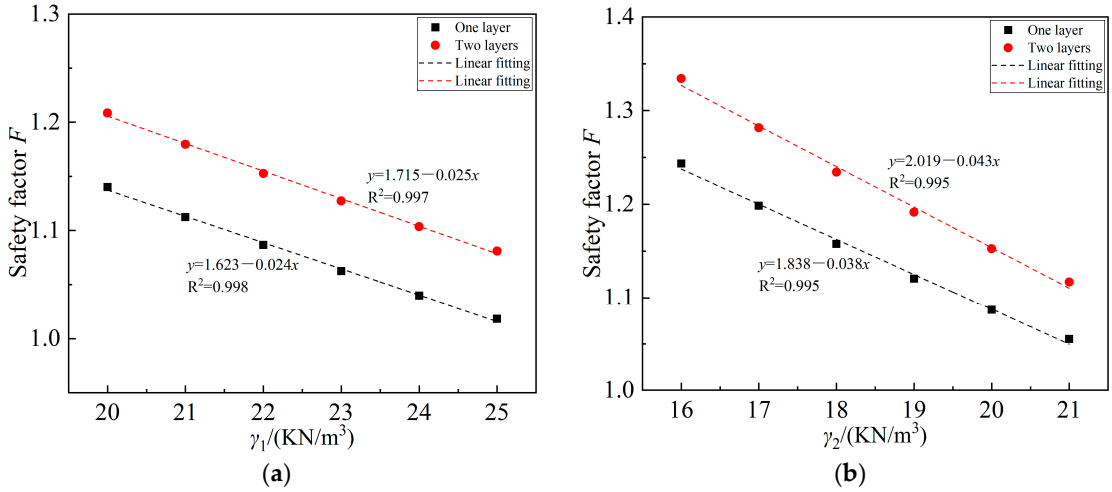

Figure 10. Relationship between safety factor and bulk density. (**a**) Safety and bottom bulk density; (**b**) Safety and central bulk density.

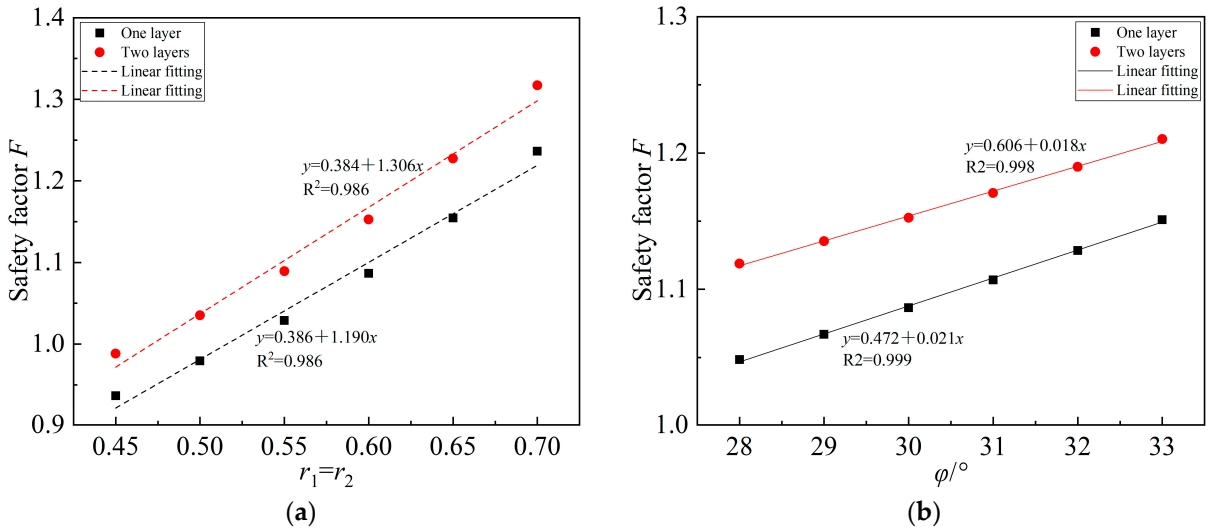

Figure 11. Relationship between safety factor and bond force ratio and internal friction angle. (**a**) Safety and bond force ratio; (**b**) Safety and internal friction angle.

Figure 8 shows the correlation between the safety factor of cemented backfill and the top load and the lateral pressure coefficient of the non-cemented backfill on the rear wall. As depicted in the figure, the safety factor decreases with the increase of the top load and lateral pressure coefficient, and the correlation between them is a linear function. With the increase of the top load, the overall downward force of the cemented backfill is increased, such that the trend of sliding downward along the wedge-shaped sliding surface is increased, the risk of instability is elevated, and the safety factor is reduced. As the lateral pressure coefficient is increased, the horizontal resultant force acting on the cemented backfill is enhanced, and the sliding trend of the wedge-shaped sliding body is also elevated, resulting in a decreased safety factor.

Figure 9 shows the correlation between the safety factor and the cohesion of the bottom and middle layers of the cemented backfill. As depicted in the figure, the safety factor increases with the increase of bottom cohesion and middle cohesion, and the correlation between the safety factor and cohesion is also a linear function. The cohesion at the bottom and middle is increased. Thus, the bonding strength between the fine particles within the cemented backfill is improved, the ability to resist instability and failure is enhanced, and the safety factor is increased.

Figure 10 illustrates the correlation between the safety factor and the bulk density of the bottom layer and the middle layer of the cemented backfill. As depicted in the figure, the safety factor decreases with the increase in unit weight, and the correlation between them is also a linear function. With the rise of the bulk density, the overall mass of the wedge-shaped sliding body is increased, and its self-gravity is elevated as well. The total downward force of the wedge-shaped sliding body is enhanced, and the downward component along the sliding surface is also increased. The sliding trend tends to be increased, whereas the safety factor is decreased.

Figure 11 presents the correlation between the safety factor of the cemented backfill and the bonding force ratio of the sidewall surrounding rock, as well as the friction angle within the cemented backfill. As depicted in the figure, the safety factor is increased with the elevation of the bonding force ratio and the internal friction angle, while they display a linear functional relationship. With the rise of the bonding force ratio, the frictional force between the surrounding rock of the sidewall and the wedge-shaped sliding body is enhanced. The upward force of the wedge-shaped sliding body is enhanced, the downward component along the sliding surface is reduced, the sliding trend declines, and the safety factor increases. If the friction angle within the cemented backfill is elevated, the equivalent increase in the friction coefficient between the fine particles within the cemented backfill

will lead to enhanced overall anti-failure ability, decreased sliding trend, and increased safety factor.

3.3. Sensitivity Analysis of Influencing Factors

The degree of effect of the respective parameter on the displacement change of the roadway and the order of primary and secondary factors varies. Moreover, due to the different dimensions of different types of parameters, there is no commonality among the parameters, making it difficult to directly determine the order of primary and secondary factors affecting the displacement change. Thus, the above-mentioned parameters can be normalized to dimensionless intervals according to a standard and then compared and analyzed. Dimensionalize the respective parameter according to the following equation [28]:

$$M = \frac{\Delta S / S}{\Delta p / p} \times 100\% \tag{25}$$

where M denotes the sensitivity of the factor; ΔS represents the change in tunnel displacement caused by parameter changes; S expresses the displacement value of the roadway under a certain benchmark parameter; Δp is the parameter variation; and p represents the reference value of the parameter. The benchmark value in this study is taken as the minimum value of the respective parameter interval.

Figure 12 shows the degree of effect of a wide variety of parameters on the safety factor. As depicted in the figure, the cohesion of the bottom layer of the cemented backfill exerts the maximum effect on the safety factor, with a sensitivity of up to 122%. The top load has the minimum effect on the safety factor, with a sensitivity of only 20%. The degree of effect of the respective parameter on the safety factor follows descending order of bottom cohesion > lateral pressure coefficient > bonding force ratio > central bulk density > bottom bulk density > internal friction angle > central cohesion > top load.

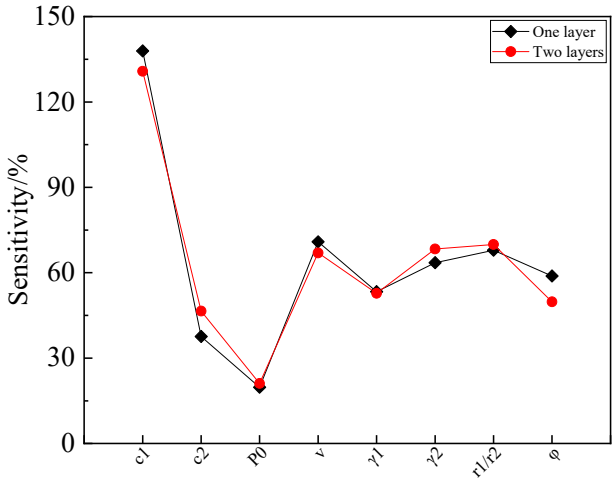

Figure 12. Variation diagram of parameter sensitivity.

4. Discussion

As indicated by the analysis in Section 2, three types of failure exist along the sliding surface of the wedge-shaped sliding body of the cemented backfill. The sliding surface is located in the first layer and passes through two layers while passing through three layers. The safety factor models for the three types of damage built separately have complex calculation equations and numerous factors, such that these models cannot be easily applied to the stability calculation of on-site handover backfill. The analysis in Section 3.1 suggests that the damage types are mainly the first two, the effect is mainly eight factors, and a good linear function relationship exists between the respective factor and the safety factor. Accordingly, consider simplifying the regression analysis of the safety factor calculation

model and using SPSS software to establish a linear regression equation between the safety factor and eight factors:

$$F_1 = -0.136 + 1.160r + 4.303c_1 + 1.223c_2 + 0.020\varphi - 3.345v - 0.025\gamma_1 - 0.037\gamma_2 - 0.908P_0 \quad (26)$$

$$F_2 = -0.052 + 1.271r + 4.315c_1 + 1.639c_2 + 0.018\varphi - 3.331v - 0.026\gamma_1 - 0.042\gamma_2 - 1.028P_0 \quad (27)$$

where F_1 and F_2 are the safety factor calculation equations for the first and second failure types, respectively.

Table 2 lists the regression analysis results. The regression results show that the multiple correlation coefficients R^2 are all greater than 0.99, suggesting a high degree of fitting. The standard errors are 0.0077 and 0.0085, both close to 0, suggesting that the fitting equation error is very small. The significance F value of both is significantly lower than 0.05, suggesting that the regression equation has a significant effect.

Table 2. Statistical table of regression results.

Safety Factor Calculation Equations	R^2	Standard Error	Significance /*F*
F_1	0.9927	0.0077	0.0001
F_2	0.9922	0.0085	0.0001

Figure 13 illustrates the intuitive degree of agreement between the safety coefficient calculated by the regression equation and the safety coefficient calculated by the model equation. Through comparative analysis of 48 sample data, it can be seen that the red curve and black curve are highly consistent, and the development trend is consistent. Intuitively, the calculation results of the regression equation are very close to the calculation results of the model equation.

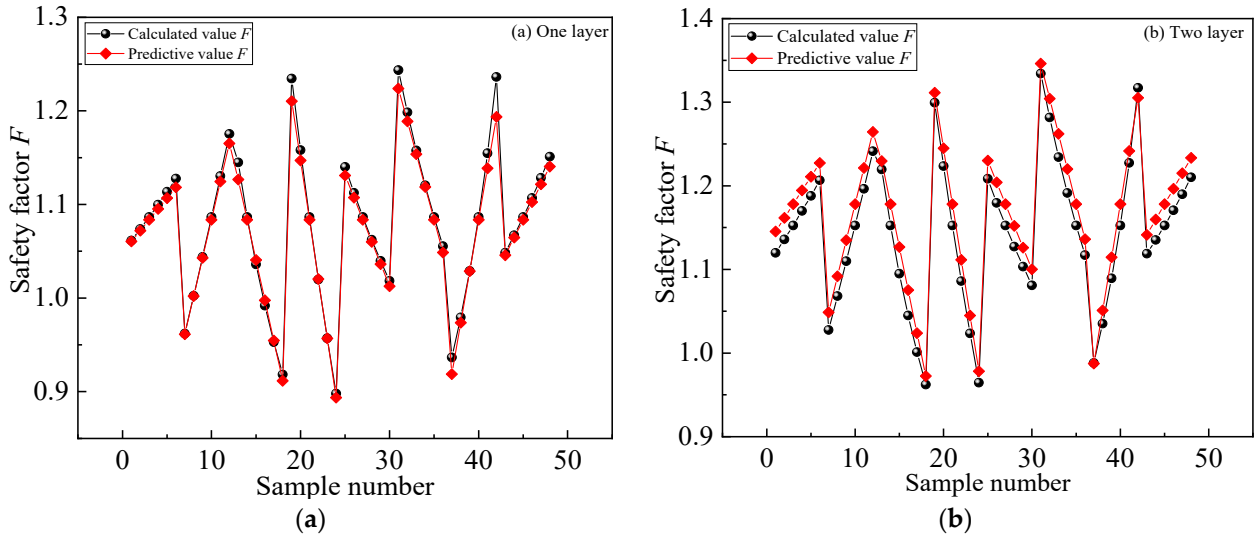

Figure 13. Analysis of the consistency between the results of regression equation and model equation. (**a**) One layer; (**b**) Two layer.

Figure 14 presents the error range between the calculation results of the regression equation and the model equation. From the figure, it can be seen that the error range of both calculation results is distributed within 10%, suggesting that the overall error is very small and the regression results are very close.

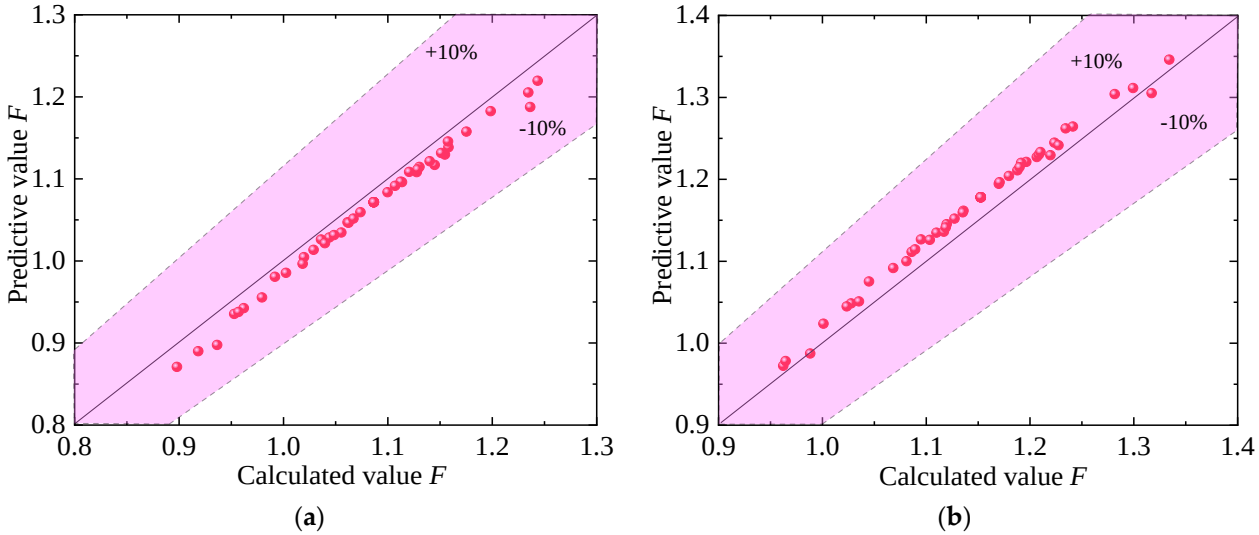

Figure 14. The error between the result of regression equation and that of model equation. (**a**) One layer; (**b**) Two layer.

To quantitatively analyze the error of regression equation settlement results, mean square error (MSE), root mean square error (RMSE), mean absolute error (MAE), and mean absolute percentage error (MAPE) are introduced to evaluate the regression results. The evaluation results are shown in Table 3.

$$MSE = \frac{\sum_{i=1}^{N} (F_y - F_j)^2}{N} \tag{28}$$

$$RMSE = \sqrt{\frac{\sum_{i=1}^{N} (F_y - F_j)^2}{N}} \tag{29}$$

$$MAE = \frac{\sum_{i=1}^{N} |F_y - F_j|}{N} \tag{30}$$

$$MAPE = \frac{1}{N} \sum_{i=1}^{N} \left| \frac{F_y - F_j}{F_y} \right| \times 100\% \tag{31}$$

Table 3. Evaluation of safety factor *F* regression prediction results.

Sliding Surface Position	MSE	RMSE	MAE	MAPE/%
Located in the first layer	0.0004	0.0209	0.0198	1.88
Located in the second layer	0.0005	0.0227	0.0219	1.88

As depicted in Table 3, MSE is significantly lower than 0.1, RMSE is significantly lower than 0.2, MAE is significantly lower than 0.2, MAPE is significantly lower than 15%, and the average absolute error percentage of all results is lower than 5%. From this, it can be seen that considering the effect of eight factors, SPSS software was used to conduct multiple linear regression analysis on the safety coefficient. The regression results were highly close to the practical calculation results, and the regression model was reasonable and reliable, which can be directly used for the stability calculation and analysis of on-site cemented backfill.

5. Conclusions

(1) Given the layering effect, lateral pressure on the back wall non-cemented backfill, top load, and frictional bonding of the side wall surrounding rock, a sliding instability model for layered cemented backfill is built in accordance with the complex occurrence environment of cemented backfill. Different structural parameters of the mining area suggest that there are three scenarios where the sliding surface is located: in the first layer, passing through two layers, and passing through three layers.

(2) Compared with other scholars' models, the results suggest that Zhang et al. [17] considered the frictional effect of non-cemented backfill on the rear wall. Li et al. [10] ignored the lateral pressure effect of non-cemented backfill on the rear wall, resulting in a higher safety factor than in this study. However, Liu et al. [16] ignored the slope toe distance of the sliding surface, resulting in a lower safety factor compared with this study. Different models have different research backgrounds and focuses, resulting in differences in safety factors, such that the correctness of the model in this study can be partially verified under specific conditions.

(3) The safety factor of cemented backfill is decreased with the increase of the top load, lateral pressure coefficient, and unit weight and increases with the increase of cohesion and cohesive force ratio. The safety factor is subjected to a linear functional relationship with the respective factor. The order of effect of the respective parameter on the safety factor is bottom cohesion > lateral pressure coefficient > bonding force ratio > central bulk density > bottom bulk density > internal friction angle > central cohesion > top load.

(4) Through the SPSS software regression analysis, a simplified multiple linear regression equation is built between the safety factor and a wide variety of factors. The calculated results of the regression equation are significantly consistent with the model results, and all error evaluation indicators fall into the effective range. The regression model is reasonable and reliable and can be applied to the stability analysis of on-site cemented backfill.

Author Contributions: J.W. and Q.Y. analyzed the experimental data and initiated the writing of the paper; G.W. and D.T. modified the manuscript. All authors have read and agreed to the published version of the manuscript.

Funding: This research was supported by the National Natural Science Foundation of China (Grant No. 52274109) and the fundamental research funds for the central universities (FRF-TP-22–113A1).

Data Availability Statement: Where no new data were created.

Acknowledgments: The experimental works described in this study were conducted at the Key Laboratory of High-Efficient Mining and Safety of Metal Mines of the Ministry of Education at the University of Science and Technology Beijing. The authors gratefully acknowledge the staff and students at the laboratory for technical help during testing.

Conflicts of Interest: The authors declare no conflict of interest.

References

1. Cao, S. *Research on Structural Characteristics and Dynamic Effects of Cemented Tailings Backfilling and Its Application*; University of Science and Technology Beijing: Beijing, China, 2017.
2. Wang, J. *Research and Application of Damage and Failure Evolution Mechanism and Strength Model of Layered Cemented Tailings Backfill*; University of Science and Technology Beijing: Beijing, China, 2021.
3. Kang, P.E.; Li, X.B.; Wan, C.C.; Peng, S.Q.; Zhao, G.Y. Safe mining technology of undersea metal mine. *Trans. Nonferrous Met. Soc. China* **2012**, *22*, 740–746.
4. Zhang, C. Application Foreground of Open Stoping Afterwards Back-filling Mining Method in Metallic Mines. *Met. Mine* **2009**, *11*, 257–260.
5. Weidong, R.E.; Yuqian, F.A. Study on Optimization of Mining Sequence in Intensive Mining with Sublevel Open Stope and Subsequent Filling. *Met. Mine* **2020**, *6*, 167–171.
6. Yang, Z.; Zhai, S.; Gao, Q.; Li, M. Stability analysis of large-scale stope using stage subsequent filling mining method in Sijiaying iron mine. *J. Rock Mech. Geotech. Eng.* **2015**, *7*, 87–94. [CrossRef]

7. Wang, J.; Fu, J.; Song, W. Mechanical properties and microstructure of layered cemented paste backfill under triaxial cyclic loading and unloading. *Constr. Build. Mater.* **2020**, *257*, 119540. [CrossRef]
8. Wang, J.; Song, W.D.; Tan, Y.Y.; Fu, J.X.; Cao, S. Damage constitutive model and strength criterion of horizontal stratified cemented backfill. *Rock Soil Mech.* **2019**, *40*, 1731–1739.
9. Shuai, C.; Gaili, X.; Song, W. Experimental research on mechanical properties of combined cemented tailings backfill and its application. *J. Min. Saf. Eng.* **2019**, *36*, 601–608.
10. Fan, J.; Rowe, R.K. Piping of silty sand tailings through a circular geomembrane hole. *Geotext. Geomembr.* **2022**, *50*, 183–196. [CrossRef]
11. Fan, J.Y.; Rowe, R.K. Seepage through a circular geomembrane hole when covered by fine-grained tailings under filter incompatible conditions. *Can. Geotech. J.* **2022**, *59*, 410. [CrossRef]
12. Fan, J.Y.; Rowe, R.K.; Brachman, R.W.I. Compressibility and permeability of sand-silt tailings mixtures. *Can. Geotech. J.* **2022**, *59*, 1348. [CrossRef]
13. Li, L.; Aubertin, M. A modified solution to assess the required strength of exposed backfill in mine stopes. *Can. Geotech. J.* **2012**, *49*, 994–1002. [CrossRef]
14. Li, L.; Aubertin, M. Numerical Investigation of the Stress State in Inclined Backfilled Stopes. *Int. J. Geomech.* **2009**, *9*, 52–62. [CrossRef]
15. Li, L. Analytical solution for determining the required strength of a side-exposed mine backfill containing a plug. *Can. Geotech. J.* **2014**, *51*, 508–519. [CrossRef]
16. Mitchell, R.J.; Olsen, R.S.; Smith, J.D. Model studies on cemented tailings used in mine backfill. *Can. Geotech. J.* **1982**, *19*, 14–28. [CrossRef]
17. Jahanbakhshzadeh, A.; Aubertin, M.; Li, L. Three-dimensional stress state in inclined backfilled stopes obtained from numerical simulations and new closed-form solution. *Can. Geotech. J.* **2018**, *55*, 810–828. [CrossRef]
18. Xiaocong, G.L. Models of three-dimensional arching stress and strength requirement for the backfill in open stoping with subsequent backfill mining. *J. China Coal Soc.* **2019**, *44*, 1391–1403.
19. Guangsheng, L. *Required Strength Model of Cemented Backfill with Research on Arching Mechanism Considering Backfill-Rock Interaction*; University of Science and Technology Beijing: Beijing, China, 2017.
20. Changguang, Z.; Mingming, C.; Hang, Q. A unified solution for calculating mine backfills considering the backfilling order and the back wall cohesion. *Chin. J. Rock Mech. Eng.* **2019**, *38*, 226–236.
21. Smith, J.D.; De Jongh, C.L.; Mitchell, R.J. Large scale model tests to determine backfill strength requirements for pillar recovery at the Black Mountain Mine. In Proceedings of the International Symposium on Mining with Backfill, Lulea, Sweden, 7–9 June 1983; pp. 413–423.
22. Liu, G.S.; Li, L.; Yang, X.C.; Guo, L. Required strength estimation of a cemented backfill with the front wall exposed and back wall pressured. *Int. J. Min. Miner. Eng.* **2018**, *9*, 1–20. [CrossRef]
23. Zhang, P.; Gao, Q.; Wen, Z.J.; Zhang, T. Influencing Factors on Backfill Strength and a Combined Strength Prediction Model. *J. Northeast. Univ.* **2021**, *42*, 232–241.
24. Yin, S.H.; Liu, J.M.; Shao, Y.J.; Zhang, H.; Armelle, B.; Kou, Y. Influence rule of early compressive strength and solidification mechanism of full tailings paste with coarse aggregate. *J. Cent. South Univ.* **2020**, *51*, 478–488.
25. Liu, G.S.; Li, L.; Yang, X.C.; Guo, L. Numerical analysis of stress distribution in backfilled stopes considering interfaces between the backfill and rock walls. *Int. J. Geomech.* **2017**, *17*, 06016014. [CrossRef]
26. Liu, G.S.; Li, L.; Yang, X.C.; Guo, L. A numerical analysis of the stress distribution in backfilled stopes considering nonplanar interfaces between the backfill and rock walls. *Int. J. Geotech. Eng.* **2016**, *10*, 271–282. [CrossRef]
27. Yajuan, H.; Junhai, Z.; Wenxiu, T. Calculation of vertical earth pressure of rigidity structures based on two shear unified strength theory. *J. Archit. Civ. Eng.* **2008**, *25*, 107–110.
28. Jianxin, F.; Weidong, S.; Yuye, T. Influence degree analysis of rock mass' mechanical parameters on roadway's deformation characteristics. *J. Zhejiang Univ* **2017**, *51*, 2365–2382.